Influence of Eddy Current Losses in Non-Superconducting Layers of HTS in Superconducting Electrical Machines

Runar Mellerud, *Graduate Student Member, IEEE*, Christian Hartmann, *Member, IEEE*, Casper Leonard Klop and Jonas Kristiansen Nøland, *Senior Member, IEEE*

***Abstract*—Superconducting electrical machines using high-temperature superconductors (HTS) are currently designed without considering losses in the non-superconducting (non-SC) substrate, silver, and copper layers of the HTS. However, alternating magnetic fields induce eddy current losses in these layers, which cannot be overlooked for certain operating temperatures and frequencies. This paper addresses these losses for a full-scale 2.5 MW aviation motor with an HTS armature winding. Using a multilayer *H*-*A*-formulated model, the magnitude of the eddy current losses are estimated and compared to the total HTS losses for frequencies between 50 and 500 Hz and temperatures between 25 and 60 K. The results show that eddy current losses are negligible for high HTS temperatures and low frequencies. However, at high frequencies and low temperatures these losses were found to represent a significant share of the total, meaning that while they can be neglected for low-speed machinery, they must be considered for power-dense machinery, particularly if the planned cooling method involves liquid hydrogen (LH_2) temperatures. Finally, the work illustrates how to analyze these losses and can give designers insights related to the influence of several design variables, such as the external field, tape height, and copper purity.**

***Index Terms*—AC losses, copper stabilizer, eddy current losses, HTS, multilayer, superconducting machines**

I. Introduction

High-temperature superconductors (HTS) can substantially reduce volume, weight, and losses in electrical machinery. Therefore, the advancement of this technology is of high priority among researchers worldwide [1]. However, when exposed to AC currents and/or fields, HTS experience losses that must be removed at cryogenic temperatures. This cryogenic cooling is challenging and will outweigh the benefits gained from the HTS if the losses are too high [2], [3]. Therefore, an accurate estimation of the AC losses is of key importance when designing the cooling system and assessing the viability of a proposed machine design.

HTS AC losses can be divided into four categories [4]:

1) Hysteresis losses in the superconducting (SC) layer;
2) Eddy current losses, caused by induced currents in the non-superconducting (non-SC) metal parts of a superconducting tape;
3) Coupling losses, caused by currents coupling two or more superconducting filaments/tapes; and,
4) Ferromagnetic losses, caused by hysteresis cycles in the case of magnetic materials.

Currently, most numerical models only consider hysteresis losses in the SC layer, neglecting the other loss components. This assumption holds for the coupling and ferromagnetic losses when each tape is electrically insulated and has a non-magnetic substrate. However, non-SC layer eddy current losses cannot be neglected for high-frequency fields and currents and can even exceed the SC layer hysteresis losses [5], [6]. Since the power of electrical machinery scales with the rotational speed, higher power densities are achievable with high frequencies. It is, therefore, necessary to find estimations of the HTS eddy current losses for these high-speed machines.

Zhang *et al.* (2020), Ma *et al.* (2020), Kails *et al.* (2020), and Musso *et al.* (2021) have previously estimated the eddy current losses in the HTS non-SC layers for single HTS tapes [6]–[9]. Moreover, Zhang *et al.* (2020) reported similar results for pancake and racetrack coils in air [10]. However, the authors have not found any work estimating these losses for large-scale applications such as electrical machines, where the electric steel and adjacent tapes will heavily influence the magnetic field across the HTS. Furthermore, previous works modeled the copper with a constant resistivity at 77 K, not investigating the influence of the temperature on the eddy losses. Therefore, this paper aims to evaluate the non-SC layer eddy current losses for an electrical machine with an HTS armature designed in [11]. We will assess which parameters the losses depend on and evaluate under which conditions they are too high to neglect. Using the mixed *H*-*A*-formulation [12], losses in the non-SC layers are found based on the multilayer approach similar to the ones outlined by Ma *et al.* (2020) and Zhang *et al.* (2020) [6], [7].

The rest of the paper is structured as follows: Section II describes the methods and models used in the analysis; Section III presents the main results, showing how the HTS eddy current losses vary within each slot and how they are impacted by temperature and frequency variations; Section IV provides a sensitivity study, investigating the impact of varying selected design parameters; Section V gives a critical discussion of assumptions and weaknesses in the analysis; finally, Section

Manuscript submitted XXXXXXX, 2024; revised XXXXXXX, 2024; accepted XXXXXXXXXX, 2024. Date of publication XXXXXXXXXX, 2024. *(Corresponding author: Runar Mellerud).*

R. Mellerud, C. L. Klop and J. K. Nøland are with the Department of Electric Energy, Norwegian University of Science and Technology (NTNU), Trondheim, 7491 Norway.

C. Hartmann is with the Institute for Energy Technology, Halden, Norway, and the Department of Electric Energy, Norwegian University of Science and Technology (NTNU), Trondheim, 7491 Norway.

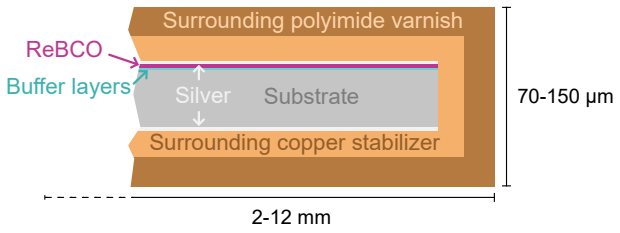

Fig. 1. Typical multilayer cross-section of a ReBCO tape with polyimide varnish. Notice that the HTS studied in this work have a copper layer completely surrounding the other layers. The polyimide varnish, substrate, silver and buffer layers were modeled as air in the analysis.

VI concludes the work.

II. Model Description

A. Multilayer Model

The typical cross-section of a ReBCO HTS is shown in Fig. 1. In this work, the following thicknesses were assumed for each layer of the ReBCO tape:

1) $15\,\mu$m surround polyimide varnish;
2) $12\,\mu$m surround copper stabilizer;
3) $2\,\mu$m silver layers;
4) $2\,\mu$m ReBCO layer; and,
5) $50\,\mu$m substrate.

Geometrically, the superconducting ReBCO layer constitutes a small part of the tape, but since this is where most of the current flows, it is usually the only layer considered in electromagnetic models. In this work, the ReBCO and copper layers were modeled explicitly with the multilayer modeling method in the H-formulation, as described in [6], [7]. Initial studies suggested that losses in the silver and substrate were negligible, like in [7], [8], and to save computation time, these layers were omitted in the analysis. In this paper, the tape transport current (I_t) was applied as a pointwise constraint in the H-formulation for each tape, as the current density (J) integrated over the ReBCO and copper layer cross-sectional surfaces (S_{ReBCO} and S_{cu}):

$$I_t = \iint_{S_{\mathrm{ReBCO}}} J\,dS + \iint_{S_{\mathrm{cu}}} J\,dS. \tag{1}$$

In the two-dimensional (2D) modeling, these layers are assumed to be perfectly coupled, not including three-dimensional (3D) effects or resistance between the layers. The current sharing between the different layers means that some of the non-SC layer losses are strictly transport losses, not magnetizing eddy current losses.

1) ReBCO layer: The resistivity of the ReBCO-layer is modeled according to the E-J power law:

$$\rho_{ReBCO} = \frac{E_c}{J_c(\mathbf{B}_{ext})}\left(\frac{|J|}{J_c(\mathbf{B}_{ext})}\right)^{n(\mathbf{B}_{ext})-1}, \tag{2}$$

where $E_c = 10^{-4}$ V m^{-1}, J is the current density, and n is the power-law index. The critical current density (J_c) and the power-law index (n) are dependent on the magnitude and angle of the external field ($\mathbf{B}_{ext}$), modeled with the same curve fits as in [11], based on experimental data for the Shanghai Superconductor low-field, high-temperature 2G HTS, from the Robinson database [13], [14].

TABLE I
Copper resistivities (ρ) used for different copper purities (RRR) and temperatures (Based on data from [16]).

T	ρ_{RRR20}	ρ_{RRR50}
25 K	0.760 nΩm	0.335 nΩm
30 K	0.798 nΩm	0.358 nΩm
40 K	0.977 nΩm	0.521 nΩm
50 K	1.300 nΩm	0.836 nΩm
60 K	1.730 nΩm	1.290 nΩm

2) Copper layer: Eddy current losses in a material are generally inversely proportional to its electrical resistivity. For metallic conductors, the resistivity decreases with temperature. This relationship depends on the material purity, represented by the residual-resistance ratio (RRR). According to Bonura *et al.* (2014), the HTS copper RRR is between 14 and 61, depending on the manufacturer [15]. Based on the corresponding copper resistivity given in Table I, it is clear that this temperature dependency is far too large to neglect.

3) Loss estimation: The volumetric loss density (p) was calculated as the product of the electric field ($\mathbf{E}$) and the current density ($\mathbf{J}$):

$$p = \mathbf{E}\cdot\mathbf{J}. \tag{3}$$

To find the instantaneous losses in each layer, the volumetric loss density was integrated over their respective cross-sections:

$$P_{layer}(t) = \iint_{S_{layer}} p\,dS. \tag{4}$$

The time-averaged losses were found by integrating over the second half period:

$$P_{layer} = \frac{2}{T}\int_{T/2}^{T} P_{layer}(t)\,dt \tag{5}$$

B. Machine Model Implementation

An aviation motor designed by Mellerud *et al.* (2023) [11] was used in this paper's case study to evaluate non-SC losses in the HTS armature. However, an important design alteration has been made. The model developed by Otten *et al.* (2020) [17] indicated that coupling losses in the non-insulated Roebel cable could be high since the coupling losses scale with the square of the frequency and amplitude of the magnetic fields [18]. Hence, tapes in the same turn should be insulated from one another under these conditions, for example, with a polyimide varnish coating [19]. Whereas a Roebel cable with interstrand insulation could be an alternative, its advantages relative to tape stacks are minimal while being more complicated to manufacture. Therefore, the 4 mm wide Roebel cable was replaced by stacks of 4 mm wide tapes with polyimide varnish for intertape insulation. Due to the extra tape height from the polyimide varnish, the slot height and, hence, the

TABLE II
KEY MACHINE PARAMETERS.

Nominal power	2.5 MW
electrical frequency	333 Hz
Phase voltage	421 V
Phase current	683 A
Number of slots	24
Number of poles	8
Air gap diameter	260 mm
Active length	240 mm
Active weight	95.5 kg
Number of turns	14
Tapes per turn	9
Tape width	4 mm
Tape height	110 μm
ReBCO layer height	2 μm
Copper stabilizer height	12 μm
Tape peak current	107.3 A
Tape critical current @ 40 K, s.f.	1017 A

outer stator diameter was increased by 1 mm, resulting in the key machine parameters given in Table II.

For the given winding configuration, HTS AC losses in each slot are equal, but phase shifted, and analysis of only one slot is sufficient to get losses representative for the entire machine. Therefore, the HTS tapes in the slot with phase B+ were modeled explicitly with the *H*-formulation, while the rest of the model was solved with the *A*-formulation, using the mixed *H*-*A* formulation developed by Brambilla *et al.* (2018) where the boundary between the two formulations is implemented by weak contributions [12].

Several efforts were made to reduce the computational burden of solving the multilayer *H*-*A*-formulated machine model. With antiperiodic boundary conditions, symmetry was used to model only one eight of the entire machine, corresponding to one rotor pole and three slots. Further, the Halbach array rotor pole was modeled with 36 static segments with time-varying excitation as described in [20], allowing a rotating rotor field while avoiding a moving mesh, as illustrated in Fig. 2. To obtain initial convergence, the current and the rotor magnetization were increased from zero using a ramp function. Still, for one electrical period, this resulted in computation times of approximately 19 hours on a Dell Poweredge C6520 server node on NTNU's HPC cluster [21].

Saturation in the electric steel was accounted for by implementing the field-dependent relative permeability of Vacoflux 50. Similarly to Mellerud *et al.* (2023) [11], the perfectly sinusoidal current was set in the q-axis, and the HTS stacks were tilted optimally relative to the slot leakage flux, meaning that the tapes are approximately parallel to the magnetic field.

Simulations showed that while HTS AC losses were quite sensitive to the number of mesh elements along the tape width, the number of elements along the copper height barely influenced copper losses. Therefore, a mapped mesh with 80 elements along the tape width with a gradient distribution with an element ratio of 12 and exponential growth rate was chosen for each tape, while two elements along the height of each copper layer were found to give satisfactory accuracy. Fig. 3 depicts the resulting mesh for one coilside (7 turns).

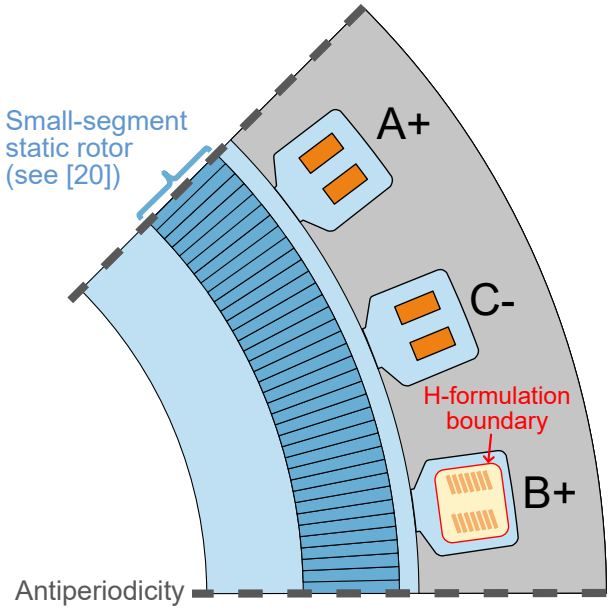

Fig. 2. Overview of machine model. The Halbach rotor pole is represented by 36 static segments with a time-varying excitation, as described in [20]. In the slot with phase B+, the HTS are modeled as multilayer tapes with the H-formulation. The rest of the model is modeled with the A-formulation.

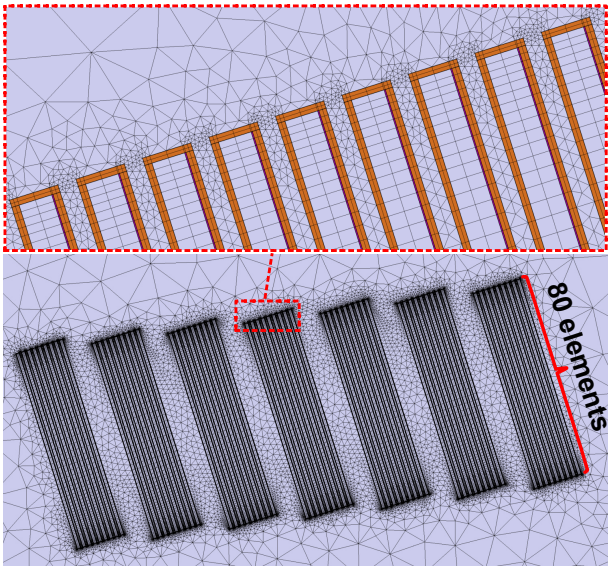

Fig. 3. Mesh of one coilside (7 turns), with 80 elements along the tape width. Notice the denser mesh distribution towards the edges.

C. Formulation Comparison and Verification

To verify the modeling, the SC layer hysteresis losses were compared with losses from an *H*-*A*-formulated model only considering the SC layer, and two *T*-*A*-formulated models: one with linear discretization in *T* and *A* (1+1), and one with linear *T* and quadratic *A* discretization (1+2). Since the *T*-*A* formulation does not consider non-SC layers, these are omitted from the comparison, only focusing on SC layer hysteresis losses. As shown in Table III, the models gave similar SC layer losses.

In cases where non-SC layer losses are negligible, the *T*-*A*-formulation is recommended due to ease of implementation;

TABLE III
SC LAYER HYSTERESIS LOSSES AND COMPUTATION TIMES OF THE GIVEN MODEL WITH SELECTED FORMULATIONS FOR ONE ELECTRICAL PERIOD AT 333 Hz AND 40 K, WITH EQUAL SOLVER PARAMETERS AND MESH DISTRIBUTION ALONG THE TAPE WIDTH

	H-A-formulation		*T-A-formulation*	
	Multilayer	SC layer only	1+1	1+2
SC layer losses	93.81 W/m	93.74 W/m	92.84 W/m	93.38 W/m
Computation time	18 h 59 min	11 h 44 min	4 h 11 min	13 h 58 min

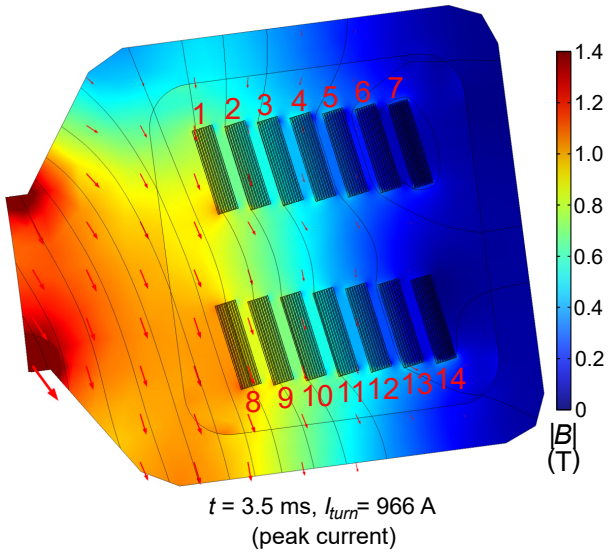

Fig. 4. Slot flux at peak current in phase B+. The turns are labeled in red for convenience.

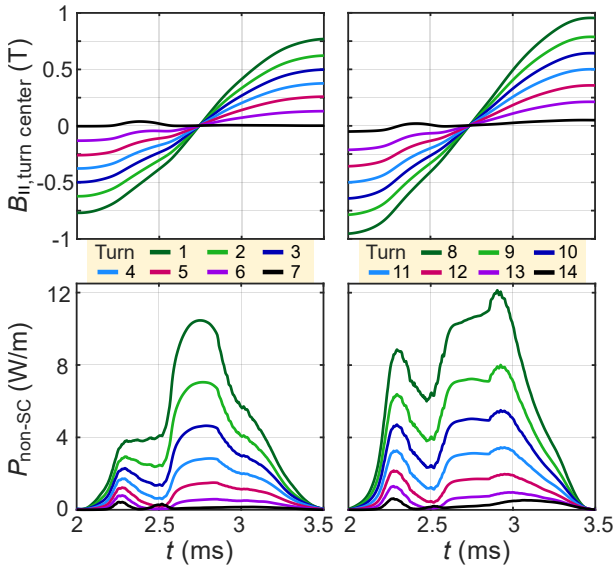

Fig. 5. Magnetic flux density in the turn center of each turn, parallel to the tape orientation (top) and instantaneous eddy current losses in each turn (bottom).

the HTS current can be applied with two Dirichlet conditions compared to numerous integrations and pointwise constraints in the *H-A*-formulation, and it allows the use of COMSOL's built-in material properties and the *Magnetic fields* interface for the *A*-formulation.

D. Model Limitations

Numerical estimation of eddy currents in conventional metals like copper is a common problem in computational electromagnetism, which has been under investigation since the early 1970s [4]. In this paper, the difference from conventional modeling is that, within each tape, the copper is assumed to be perfectly coupled with the SC layer, using the multilayer approach validated in [6], [7], neglecting end effects and poor connection between layers from, for example, delamination.

Because of the sensitivity of HTS AC losses relative to the magnetic field and the HTS normalized current, the eddy current loss fractions found in this paper might not be directly applicable to other machine designs.

III. Results

A. Interturn Loss Variation

Eddy current losses generally depend on the peak of the magnetic flux density squared. Fig. 4 depicts the magnetic field inside the slot at the time-instant with peak current, and hence peak slot flux according to Ampere's law. The field is slightly inclined in the rotation direction due to the q-axis current, aligning almost perfectly with the slightly tilted HTS stacks. Since the turns closest to the air gap experience the highest field, they are also expected to have higher losses. This is what is observed when plotting the field parallel to the tapes in each turn center, along with the copper losses, in Fig. 5; a lower magnetic peak flux predictably gives lower HTS eddy current losses. The same Fig. shows that the losses are largest when the field (and current) goes through zero at 2.75 ms, i.e., when the $d\Phi/dt$ is largest and when the transport current is low. This indicates that it is indeed the eddy currents that are mainly inducing the non-SC losses, not the transport current. A polynomial fit of loss data versus frequency showed that the copper losses were of a quadratic nature, further confirming the above statement.

The current and loss density in the most counterclockwise part of turn 8 is plotted in Fig. 6 for the time instance with peak losses. Here, it is clear that both the current and losses occur mainly at the side opposite to the SC layer, indicating that there are shielding current loops induced by the parallel field flowing partly in the SC layer and partly in the bottom copper layer.

B. Frequency and Temperature

To investigate the impact of the frequency and temperature on the HTS losses, the model was simulated at 50, 100, 200, 333 and 500 Hz for HTS temperatures of 25, 30, 40, 50 and

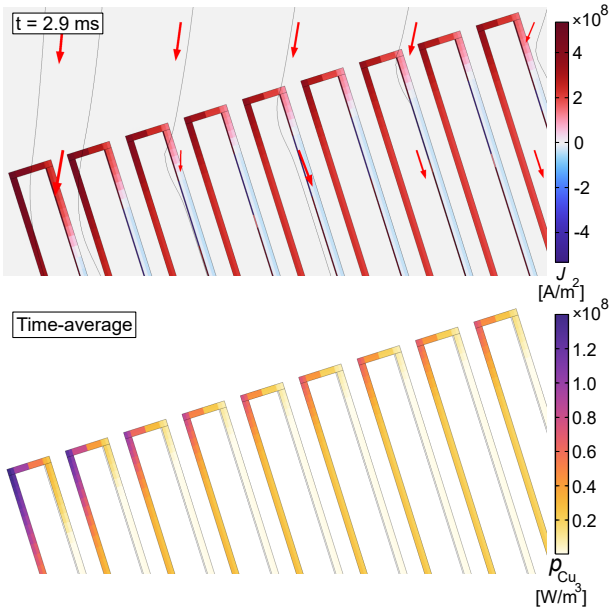

Fig. 6. 2D plot of most counterclockwise part of turn 8, showing the copper current density at the time instant of peak losses (top) and time-averaged copper loss density (bottom).

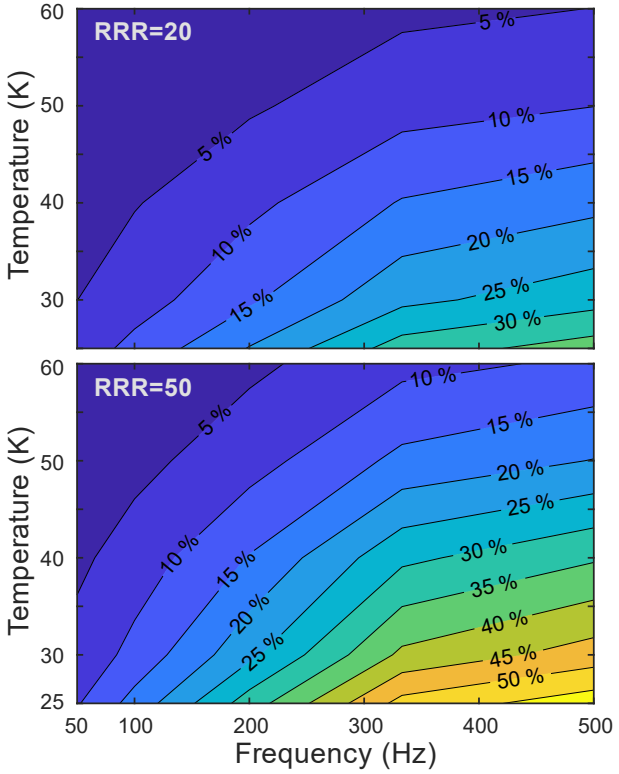

Fig. 7. Map of copper loss fraction (P_{cu}/P_{tot}) for a copper RRR=20 (top) and RRR=50 (bottom).

60 K, resulting in the map of the copper loss fraction shown in Fig. 7.

Whereas hysteresis losses are proportional to the frequency, eddy currents are proportional to the frequency squared, as shown in Table IV. Hence, copper losses are more pronounced as the frequency increases and will exceed hysteresis losses

TABLE IV
HTS LOSSES AT 40 K WHEN VARYING THE FREQUENCY FOR COPPER WITH RRR=20 AND RRR=50. SC LAYER LOSSES WERE FOUND WITH RRR=50.

f	P_{sc}	$P_{cu,RRR=50}$	$P_{cu,RRR=20}$
50 Hz	16.24 W/m	0.675 W/m	0.360 W/m
100 Hz	30.87 W/m	2.672 W/m	1.426 W/m
200 Hz	58.57 W/m	10.59 W/m	5.649 W/m
333 Hz	93.81 W/m	29.20 W/m	15.59 W/m
500 Hz	136.1 W/m	65.35 W/m	34.90 W/m

TABLE V
HTS LOSSES AT 333 HZ WHEN VARYING THE HTS TEMPERATURE FOR COPPER WITH RRR=20 AND RRR=50. SC LAYER LOSSES WERE FOUND WITH RRR=50.

T	P_{sc}	$P_{cu,RRR=50}$	$P_{cu,RRR=20}$
25 K	47.62 W/m	42.74 W/m	18.65 W/m
30 K	58.00 W/m	40.46 W/m	18.16 W/m
40 K	93.81 W/m	29.20 W/m	15.59 W/m
50 K	157.1 W/m	20.76 W/m	13.38 W/m
60 K	284.3 W/m	19.99 W/m	15.01 W/m

if the frequency gets high enough, as shown in Fig. 7 and observed by Zhang *et al.* (2020) [6]. A closer investigation of the hysteresis losses in Table IV shows that they are slightly less than proportional to the frequency. This could be because of more efficient magnetic shielding at higher frequencies.

As shown in Table V, reducing the HTS temperature has an opposite impact on losses in the SC layer and the copper layer; while it reduces hysteresis losses due to a higher critical current, it increases eddy current losses due to a higher conductivity. As illustrated in Fig. 7, this means that at temperatures above 60 K, HTS copper losses can be assumed to be negligible for most applications. However, these losses should be considered at lower temperatures, for example, in applications where the HTS are cooled by liquid hydrogen (LH_2).

The losses in Table IV and V show that a copper RRR=50 gives roughly twice as high copper losses compared to RRR=20 (less at higher temperatures), illustrating the importance of an accurate measure of the copper RRR. When comparing with the resistivities given in Table I, it is clear that the copper losses are indeed inversely proportional to the copper resistivity.

IV. Sensitivity Study

In this section, the four design parameters illustrated in Fig. 8 were varied to investigate their influence on the copper losses. Unless otherwise specified, results were found for the specified geometry at full load current with a frequency of 333 Hz, a uniform HTS temperature of 40 K, and copper RRR=50.

A. Angle of External Field

Losses were estimated when each turn was tilted clockwise by an angle (β) relative to the initial model, with the turn center being the center of rotation. Since the initial angle puts the HTS approximately in parallel with the external field (as shown in Fig. 4), β roughly corresponds to the angle between

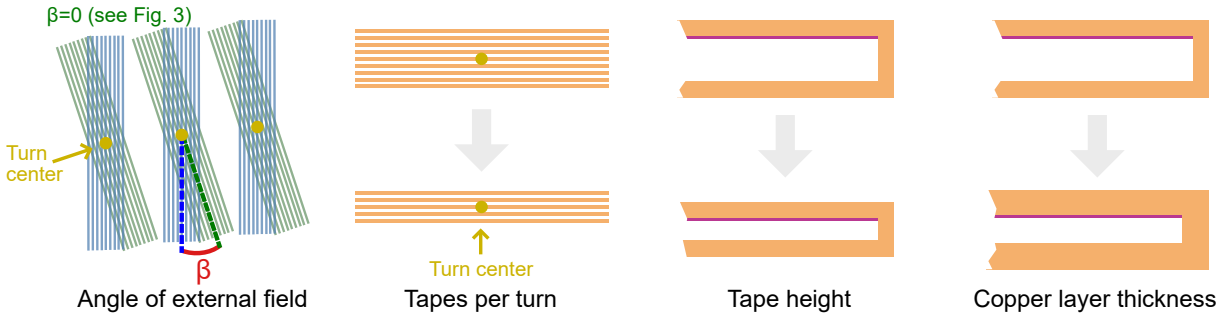

Fig. 8. Cases investigated in the sensitivity study.

TABLE VI
HTS LOSSES WHEN VARYING THE ANGLE OF THE HTS TAPES RELATIVE TO THE EXTERNAL FIELD, WHERE 0 DEG IS APPROXIMATELY PARALLEL TO THE FIELD.

β	P_{tot}	P_{cu}/P_{tot}
0 °	123.0 W/m	23.7 %
4 °	143.3 W/m	20.9 %
8 °	197.8 W/m	16.7 %
12 °	293.8 W/m	13.6 %
16 °	438.0 W/m	12.2 %
20 °	638.7 W/m	12.0 %
24 °	895.8 W/m	12.5 %

TABLE VII
HTS LOSSES WHEN VARYING THE NUMBER OF TAPES PER TURN (N_{tapes}).

N_{tapes}	$I_{peak}/I_{c,s.f.}$	P_{tot}	P_{cu}/P_{tot}
8	23.7 %	231.6 W/m	9.11 %
10	19.0 %	181.0 W/m	11.5 %
12	15.8 %	157.3 W/m	14.3 %
14	13.6 %	141.3 W/m	17.3 %
16	11.9 %	130.5 W/m	20.5 %
18	10.6 %	123.0 W/m	23.7 %
20	9.50 %	117.4 W/m	27.0 %

the external field and the HTS. The results are given in Table VI, which shows that the total losses increase rapidly with β, making it clear that the superconductors must be close to parallel with the magnetic field to avoid excessive losses. Further, the copper loss ratio is highest when the field is parallel to the HTS, as the SC layer losses are more sensitive to the field angle than the copper layer losses.

B. Number of Tapes Per Turn

Like in [11], the number of parallel coupled tapes per turn was varied while maintaining a constant turn current, effectively investigating the impact of the HTS normalized current (I/I_c) on the copper loss fraction (P_{cu}/P_{tot}). The results are presented in Table VII, where the number of tapes influences losses in the SC layer far more than in the copper layer. Hence, SC layer losses can be expected to be more dominating when the HTS normalized current is increased.

C. Tape Height

Table VIII shows how the tape height influences the HTS losses. In this analysis, the tape height was varied by reducing

TABLE VIII
HTS LOSSES WHEN VARYING THE TAPE HEIGHT (h_{tape}).

h_{tape}	P_{tot}	P_{cu}	P_{cu}/P_{tot}
110 μm	123.0 W/m	29.20 W/m	23.7 %
100 μm	114.5 W/m	21.03 W/m	18.4 %
90 μm	107.5 W/m	14.27 W/m	13.3 %
80 μm	102.1 W/m	8.93 W/m	8.75 %
70 μm	97.84 W/m	5.02 W/m	5.13 %

TABLE IX
HTS LOSSES WHEN VARYING THE COPPER LAYER HEIGHT (h_{cu}).

h_{cu}	P_{tot}	P_{cu}/P_{tot}
7 μm	114.7 W/m	18.3 %
12 μm	123.0 W/m	23.7 %
17 μm	126.6 W/m	26.2 %
22 μm	127.2 W/m	26.7 %
27 μm	125.6 W/m	26.1 %

the substrate height while keeping the tapes in place, introducing a vertical gap between the tapes. As the copper losses increase almost six-fold when going from a height of 70 μm to 110 μm, it is clear that the eddy current losses depend on the tape height and that a low tape height is beneficial. This is because the magnetic field is mostly parallel to the HTS. Analogous to laminations in an electric machine, reducing the cross-section perpendicular to the alternating field will reduce eddy currents. For this analysis, it is important to keep in mind that the polyimide varnish occupies 30 μm of the tape height.

D. Copper Layer Height

To investigate the influence of the copper layer height isolatedly, the tape height was kept constant at 110 μm by varying the substrate height. The results in Table IX show that given a constant tape height, the copper losses increase with the copper height until a point from which it stays almost constant.

V. CONCLUSION

By implementing a multilayer *H-A* formulation on a full-scale model of an aviation motor with a superconducting armature, HTS eddy current losses in non-superconducting layers were investigated in this paper. For the investigated motor design, it was shown that although non-SC layer losses are generally negligible in applications with lower frequencies

and higher HTS temperatures, they exceeded $50\,\%$ of the total HTS losses for the given design with at $25\,\mathrm{K}$, $500\,\mathrm{Hz}$ and a copper RRR=50. Hence, while only considering the SC layer hysteresis losses might give accurate loss estimations for wind power applications, eddy current losses must be considered in aircraft machinery.

The impact of certain design parameters on the eddy current loss fraction was investigated. From this perspective, it is clear that machine designers should pay close attention to HTS parameters such as copper purity since an RRR=50 gave roughly twice as high eddy current losses as an RRR=20. With a field parallel to the HTS, the tape height will also have a large impact on the copper losses, increasing almost six-fold when going from a height of $70\,\mu\mathrm{m}$ to $110\,\mu\mathrm{m}$. Lastly, the eddy current loss fractions were found to depend on the angle and magnitude of the magnetic flux, as well as the normalized current. Therefore, the loss fractions found here are not necessarily directly applicable to other machine designs.

Acknowledgements

The authors would like to express their gratitude to Robin Köster for help with modeling nonlinear steel in the *H-A* formulation, and Simon Otten for providing valuable insights and models for estimating Roebel cable coupling losses.

References

[1] K. S. Haran *et al.*, "High power density superconducting rotating machines—development status and technology roadmap," *Supercond. Sci. Technol.*, vol. 30, no. 12, p. 123002, Nov. 2017.

[2] M. Gouge, J. Demko, B. Mcconnell, and J. Pfotenhauer, "Cryogenics assessment report," 2002.

[3] C. C. Chow, M. D. Ainslie, and K. Chau, "High temperature superconducting rotating electrical machines: An overview," *Energy Rep.*, vol. 9, pp. 1124–1156, 2023.

[4] F. Grilli, E. Pardo, A. Stenvall, D. N. Nguyen, W. Yuan, and F. Gömöry, "Computation of losses in hts under the action of varying magnetic fields and currents," *IEEE Trans. Appl. Supercond.*, vol. 24, no. 1, pp. 78–110, 2014.

[5] B. Shen *et al.*, "Investigation and comparison of AC losses on stabilizer-free and copper stabilizer HTS tapes," *Physica C*, vol. 541, pp. 40–44, 2017.

[6] H. Zhang *et al.*, "Modelling of electromagnetic loss in HTS coated conductors over a wide frequency band," *Supercond. Sci. Technol.*, vol. 33, no. 2, p. 025004, Jan. 2020.

[7] J. Ma, J. Geng, W. K. Chan, J. Schwartz, and T. Coombs, "A temperature-dependent multilayer model for direct current carrying HTS coated-conductors under perpendicular AC magnetic fields," *Supercond. Sci. Technol.*, vol. 33, no. 4, p. 045007, Feb. 2020.

[8] K. Kails, H. Zhang, M. Mueller, and Q. Li, "Loss characteristics of HTS coated conductors in field windings of electric aircraft propulsion motors," *Supercond. Sci. Technol.*, vol. 33, no. 6, p. 064006, 2020.

[9] A. Musso, M. Breschi, P. L. Ribani, and F. Grilli, "Analysis of AC loss contributions from different layers of HTS tapes using the AV formulation model," *IEEE Trans. Appl. Supercond.*, vol. 31, no. 2, pp. 1–11, 2021.

[10] H. Zhang, P. Machura, K. Kails, H. Chen, and M. Mueller, "Dynamic loss and magnetization loss of HTS coated conductors, stacks, and coils for high-speed synchronous machines," *Supercond. Sci. Technol.*, vol. 33, no. 8, p. 084008, Jul. 2020.

[11] R. Mellerud, C. Hartmann, C. L. Klop, S. Austad, and J. K. Nøland, "Design of a power-dense aviation motor with a low-loss superconducting slotted armature," *IEEE Trans. Appl. Supercond.*, vol. 33, no. 8, pp. 1–13, 2023.

[12] R. Brambilla, F. Grilli, L. Martini, M. Bocchi, and G. Angeli, "A finite-element method framework for modeling rotating machines with superconducting windings," *IEEE Trans. Appl. Supercond.*, vol. 28, no. 5, pp. 1–11, 2018.

[13] S. C. Wimbush, N. M. Strickland, and A. Pantoja, "Critical current characterisation of Shanghai Superconductor Low Field High Temperature 2G HTS superconducting wire," Feb. 2022.

[14] S. C. Wimbush and N. M. Strickland, "A public database of high-temperature superconductor critical current data," *IEEE Trans. Appl. Supercond.*, vol. 27, no. 4, pp. 1–5, 2017.

[15] M. Bonura and C. Senatore, "High-field thermal transport properties of REBCO coated conductors," *Supercond. Sci. Technol.*, vol. 28, no. 2, p. 025001, Dec. 2014.

[16] N. Sanchez, "Cryogenic Properties of Copper." [Online]. Available: https://www.copper.org/resources/properties/cryogenic/#

[17] S. Otten, A. Kario, E. Demenčik, R. Nast, and F. Grilli, "Anisotropic monoblock model for computing AC loss in partially coupled roebel cables," *Supercond. Sci. Technol.*, vol. 33, no. 9, p. 094013, Jul. 2020.

[18] S. Otten, "Characterisation of REBCO roebel cables," Ph.D. dissertation, Karlsruher Institut für Technologie (KIT), 2019.

[19] J. ter Harmsel, S. Otten, M. Dhallé, and H. ten Kate, "Magnetization loss and transport current loss in rebco racetrack coils carrying stationary current in time-varying magnetic field at 4.2k," *Supercond. Sci. Technol.*, vol. 36, no. 1, p. 015011, Dec. 2022.

[20] C. Hartmann, R. Mellerud, J. K. Nøland, and R. Nilssen, "A static FEA framework for fast analysis of HTS armature windings in AC superconducting SMPM machines," *IEEE Trans. Energy Convers.*, vol. 38, no. 3, pp. 2191–2201, 2023.

[21] M. Själander, M. Jahre, G. Tufte, and N. Reissmann, "EPIC: An energy-efficient, high-performance GPGPU computing research infrastructure," *CoRR*, vol. abs/1912.05848, 2019.